Measurements of the cross-phase angle between density and electron temperature fluctuations and comparison with gyrokinetic simulations

Citation: White, A. E. et al. "Measurements of the Cross-phase Angle Between Density and Electron Temperature Fluctuations and Comparison with Gyrokinetic Simulations." Physics of Plasmas 17.5 (2010) : 056103. © 2010 American Institute of Physics

As Published: http://dx.doi.org/10.1063/1.3323084

Publisher: American Institute of Physics

Persistent URL: http://hdl.handle.net/1721.1/65841

Version: Final published version: final published article, as it appeared in a journal, conference proceedings, or other formally published context

Measurements of the cross-phase angle between density and electron temperature fluctuations and comparison with gyrokinetic simulations[a)]

A. E. White,[1,b)] W. A. Peebles,[2] T. L. Rhodes,[2] C. H. Holland,[3] G. Wang,[3] L. Schmitz,[2] T. A. Carter,[2] J. C. Hillesheim,[2] E. J. Doyle,[2] L. Zeng,[2] G. R. McKee,[4] G. M. Staebler,[5] R. E. Waltz,[5] J. C. DeBoo,[5] C. C. Petty,[5] and K. H. Burrell[5]
[1]*Oak Ridge Institute for Science and Education (ORISE), Oak Ridge, Tennessee 37831, USA*
[2]*University of California, Los Angeles, Los Angeles, California 90095, USA*
[3]*University of California, San Diego, La Jolla, California 92093, USA*
[4]*University of Wisconsin, Madison, Wisconsin 53706-1481, USA*
[5]*General Atomics, San Diego, California 92186-5608, USA*

(Received 17 December 2009; accepted 27 January 2010; published online 12 March 2010)

This paper presents new measurements of the cross-phase angle, $\alpha_{n_eT_e}$, between long-wavelength ($k_\theta \rho_s < 0.5$) density, $\tilde{n}_e$, and electron temperature, $\tilde{T}_e$, fluctuations in the core of DIII-D [J. L. Luxon, Nucl. Fusion **42**, 614 (2002)] tokamak plasmas. The coherency and cross-phase angle between $\tilde{n}_e$ and $\tilde{T}_e$ are measured using coupled reflectometer and correlation electron cyclotron emission diagnostics that view the same plasma volume. In addition to the experimental results, two sets of local, nonlinear gyrokinetic turbulence simulations that are performed with the GYRO code [J. Candy and R. E. Waltz, J. Comput. Phys. **186**, 545 (2003)] are described. One set, called the pre-experiment simulations, was performed prior to the experiment in order to predict a change in $\alpha_{n_eT_e}$ given experimentally realizable increases in the electron temperature, T_e. In the experiment the cross-phase angle was measured at three radial locations (ρ=0.55, 0.65, and 0.75) in both a "Base" case and a "High T_e" case. The measured cross-phase angle is in good qualitative agreement with the pre-experiment simulations, which predicted that $\tilde{n}_e$ and $\tilde{T}_e$ would be out of phase. The pre-experiment simulations also predicted a decrease in cross-phase angle as T_e is increased. Experimentally, this trend is observed at the inner two radial locations only. The second set of simulations, the postexperiment simulations, is carried out using local parameters taken from measured experimental profiles as input to GYRO. These postexperiment simulation results are in good quantitative agreement with the measured cross-phase angle, despite disagreements with transport fluxes. Directions for future modeling and experimental work are discussed. © *2010 American Institute of Physics*. [doi:10.1063/1.3323084]

I. INTRODUCTION

The importance of long-wavelength turbulent fluctuations in determining cross-field transport in the core of tokamak plasmas is of considerable interest to the field of magnetically confined fusion. Measurements of the cross-phase angles between different fluctuating fields, in addition to turbulence fluctuation levels, are essential for diagnosing turbulence driven transport.[1,2] The expression for cross-field energy flux, $\tilde{Q}$, due to electrostatic turbulence can be written (without species indices) as $\tilde{Q}=\langle \tilde{p}\tilde{v}_r \rangle$, in terms of fluctuations in pressure, $\tilde{p}$, and the radial component of the $E\times B$ velocity, $\tilde{v}_r$, where $\langle\ \rangle$ indicates an ensemble average. This can be expanded as

$$\tilde{Q} = \frac{3k_\theta}{2B_\phi}[n_0 \tilde{T}\tilde{\phi}\gamma_{T\phi}\sin(\alpha_{T\phi}) + T_0 \tilde{n}\tilde{\phi}\gamma_{n\phi}\sin(\alpha_{n\phi})], \quad (1)$$

which illustrates that the electrostatic turbulent cross-field energy flux depends on several turbulence parameters that can be measured: the rms levels of temperature fluctuations, $\tilde{T}$, density fluctuations, $\tilde{n}$, potential fluctuations, $\tilde{\phi}$, as well as the cross-phase angles, $\alpha_{T\phi}$ and $\alpha_{n\phi}$, and the coherencies, $\gamma_{T\phi}$ and $\gamma_{n\phi}$. Here n_0 and T_0 are the density and temperature, B_ϕ is the background magnetic field in the toroidal direction, k_θ is the wave number of fluctuations, and $\tilde{\phi}\approx -\tilde{E}_\theta/k_\theta$. Measuring all these quantities simultaneously allows for direct evaluation of turbulent electrostatic energy flux. In the edge plasma of tokamak experiments these measurements are made using Langmuir probes.[1] In the core of tokamak plasmas, simultaneous measurement of multiple fluctuating fields and cross-phase angles is difficult and has rarely been performed.[3–5] At the DIII-D tokamak,[6] a correlation electron cyclotron emission (CECE) diagnostic allows for local measurement of long-wavelength electron temperature fluctuations.[7] The availability of a beam emission spectroscopy (BES) diagnostic[8] allows for simultaneous measurement of local density fluctuations, but at a location toroidally and poloidally displaced from CECE measurement location.[9] Recently two new multichannel reflectometer systems[10,11] used for density fluctuation measurements have become available. One of the reflectometer systems has been coupled with the CECE system in order to measure $\tilde{n}_e$ and $\tilde{T}_e$, respectively, at the same toroidal, poloidal, and radial position in

[a)]Paper KI3 1, Bull. Am. Phys. Soc. **54**, 137 (2009).
[b)]Invited speaker.

the core plasma at DIII-D. The cross-phase angle between $\tilde{n}_e$ and $\tilde{T}_e$ can be measured using this new coupled reflectometer-CECE system. While the cross-phase angle $\alpha_{n_eT_e}$ does not enter directly into the turbulence-driven flux equations, comparisons of this measurement with theory and simulation provide valuable new information about the physics of turbulence driven transport associated with ion temperature gradient (ITG) and trapped electron mode (TEM) instabilities.[12] For example, the sign of $\alpha_{n_eT_e}$ could be used to identify an instability as an ion branch or electron branch mode,[13] similar to measurements of the propagation direction of turbulence in the plasma frame.[1,2] Quasilinear transport approximations include a model for the dominant mode's linear cross-phase angle that is the same as the nonlinear cross-phase angle,[14] which means that measurements of $\alpha_{n_eT_e}$ can be compared against reduced, theory-based transport models such as TGLF.[15] Measurements of the cross-phase angle also provide a new constraint on nonlinear, gyrokinetic turbulence-transport codes, such as GYRO.[16] Simultaneous measurements of the cross-phase angle, $\alpha_{n_eT_e}$, and two-field fluctuation levels, combined with experimentally inferred power flows and thermal diffusivities, will allow for comparisons at multiple levels of a "primacy hierarchy,"[17,18] which is important for rigorous testing and validation of turbulence-transport models.

The main goals of the experiments described here were to study the cross-phase angle between long-wavelength density and electron temperature fluctuations and to produce a new, comprehensive turbulence data set for future validation efforts. In this paper, we present new measurements of the cross-phase angle, $\alpha_{n_eT_e}$, between long-wavelength ($k_\theta \rho_s < 0.5$) density, $\tilde{n}_e$, and electron temperature, $\tilde{T}_e$, fluctuations in the core of DIII-D tokamak plasmas. Here k_θ is the wave number of the fluctuations and ρ_s is the ion sound gyroradius defined as $\rho_s = c_s/\Omega_{ci}$, where $c_s = \sqrt{T_e/m_i}$ and $\Omega_{ci} = eB/m_i c$. In addition to the experimental results, we describe two sets of nonlinear gyrokinetic turbulence simulations that are performed with the GYRO code.[16] One set, called the pre-experiment simulations, was performed prior to the experiment in order to predict a change in $\alpha_{n_eT_e}$ given experimentally realizable modifications to the electron temperature profile. The second set of simulations, the postexperiment simulations, is carried out in a traditional manner[18–20] using local parameters taken from measured experimental profiles as input in order to quantitatively compare with turbulence measurements. Both pre-experiment and postexperiment gyrokinetic simulations have been used for comparisons with experiment. The pre-experiment simulations predicted that $\tilde{n}_e$ and $\tilde{T}_e$ would be out of phase, $\alpha_{n_eT_e} \approx -110°$, in ITG dominant L-mode plasmas. The pre-experiment simulations also predicted that $\alpha_{n_eT_e}$ would decrease to $\alpha_{n_eT_e} \approx -70°$ when electron temperature increased by 50% ($1/L_{T_e}$ constant). The inverse gradient scale length is defined, for temperature for example, as $1/L_T = |(1/T) \times (dT/dr)|$. In the nonlinear simulations, the change in cross-phase angle is accompanied by a change from ITG turbulence to TEM turbulence as T_e increases. Neutral beam heated L-mode tokamak plasmas were used to test the new prediction for changes in cross-phase angle. Experimentally, T_e is increased using local electron cyclotron heating (ECH). The response of the cross-phase angle, $\alpha_{n_eT_e}$, is monitored at three radial locations, $\rho = 0.55, 0.65$, and 0.75. At all radii, density and electron temperature fluctuations are measured to be out of phase, and the values of the cross-phase angle is qualitatively consistent with the pre-experiment simulation results. The measured cross-phase angle decreased significantly by approximately 45° at $\rho = 0.55$ and $\rho = 0.65$ in the "High T_e" discharges that had neutral beam heating in addition to ECH. This experimentally observed change in the cross-phase angle is qualitatively consistent with the trend predicted by the pre-experiment simulations. However, at $\rho = 0.75$ the measured change in $\alpha_{n_eT_e}$ is within the experimental uncertainty. A goal for this work is to compare the two experimental cases quantitatively against postexperiment simulations at all radial locations, but at this stage only simulations for the "High T_e" case at one radius have been completed. These postexperiment simulation results are in good quantitative agreement with the measured cross-phase angle, despite disagreements with transport fluxes. Directions for future modeling and experimental work are discussed.

The remainder of this paper is organized as follows. Section II describes the pre-experiment GYRO simulations used to predict changes in $\alpha_{n_eT_e}$, Sec. III describes the coupled reflectometer and CECE diagnostics used to measure $\alpha_{n_eT_e}$, Sec. IV describes the experimental results and measured changes in $\alpha_{n_eT_e}$, Sec. V presents initial quantitative comparisons between postexperiment GYRO simulations and experimental results, and Sec. VI presents a summary of results and a discussion of ongoing and future work.

II. PRE-EXPERIMENT GYRO SIMULATIONS

One difficulty encountered in testing turbulence-transport models via direct comparison with experiment is that transport levels and fluctuation levels predicted by nonlinear gyrokinetic simulations are highly sensitive to density and temperature gradients used as input to the codes.[16,18,19] When comparisons between experiment and simulation are performed, it is usually possible to improve quantitative agreement in a single quantity at a single radial location by varying the input gradients within experimental error bars. This is attributed to the so-called "stiffness" of the transport models observed close to marginal stability.[16] Because of this sensitivity to input parameters, to critically test the codes it is important to make multilevel comparisons at several radial locations and plasma conditions. Predictions from simulations for changes in turbulence-driven transport fluxes for multiple plasma conditions are obtained using parameter scans, which typically include scans of one drive or damping term (all other parameters held fixed). As an example, the effects of safety factor and magnetic shear are considered by Ref. 21 using a large number of nonlinear GYRO simulations. These types of extensive scans usually track changes in transport fluxes, but not fluctuations. Therefore, in this project we have used fully nonlinear, pre-experiment simulations with all turbulence information included to aid in the design of dedicated validation experiments. Because these

TABLE I. Local parameters at midradius used in two pre-experiment GYRO simulations. The "Base" case parameters are from DIII-D discharge 128 913, ρ=0.5, t=1500 ms. For the "High T_e" case the input electron temperature to GYRO has been increased 50%.

Parameter	Base 128913	High T_e 128913	Change (%)
ρ	0.5	0.5	⋯
a (m)	0.62	0.62	⋯
c_s/a (kHz)	215	263	+22
n_e (10^{19} m^{-3})	2.083	2.083	⋯
T_i (keV)	0.805	0.805	⋯
T_e (keV)	0.964	1.446	+50
a/L_{n_e}	1.070	1.070	⋯
a/L_{T_i}	1.807	1.807	⋯
a/L_{T_e}	2.646	2.646	⋯
γ_{ExB} (c_s/a)	0.040	0.040	⋯
ν_{ei} (c_s/a)	0.117	0.053	−55
T_i/T_e	0.835	0.557	−33
ρ^*	0.0026	0.0032	+23
Z_{eff}	1.325	1.325	⋯
q	1.827	1.827	⋯
$\hat{s}$	0.626	0.626	⋯

pre-experiment simulations, like traditional postexperiment simulations,[16,18–20] are difficult, time consuming, and computationally expensive to carry out, we do use linear stability calculations to select target conditions and potential parameter scans in preparation for the pre-experiment nonlinear turbulence simulations. The final set of nonlinear pre-experiment scans are used to track the responses of measurable turbulence characteristics to realistic changes in plasma parameters. While this does allow for qualitative testing of predictions from basic drift wave instability models in experiments, the parameters used as input to the simulations will not be identical to the parameters actually achieved. It is important to also carry out traditional postexperiment simulations and to employ synthetic diagnostics[18,22] so that measurements of the turbulence can be directly compared with nonlinear gyrokinetic turbulence simulations.

In this work, simulations are performed using the nonlinear gyrokinetic turbulence and transport code GYRO, which is an advanced and physically comprehensive Eulerian δf code that can be run in the local limit (flux-tube) or in global mode.[16,23] The equilibrium $E\times B$ shear is included using the Waltz–Miller formulation and a Miller equilibrium model is used to account for magnetic geometry effects. For the pre-experiment parameter scans, baseline experimental L-mode parameters taken from ρ=0.5 in DIII-D discharge 128 913,[9] and a series of local, nonlinear GYRO runs were performed. These quasistationary, sawtooth-free L-mode plasma conditions provide good conditions for performing turbulence-transport simulations. Simulations done in the local limit, ρ^*=0, are in good agreement with global results in these cases.[18] Details of past simulations of 128 913 are described in detail by Ref. 18 but the local input parameters at ρ=0.5 are summarized here in Table I for reference, labeled as a "Base" case. The GYRO runs for the "Base" case showed

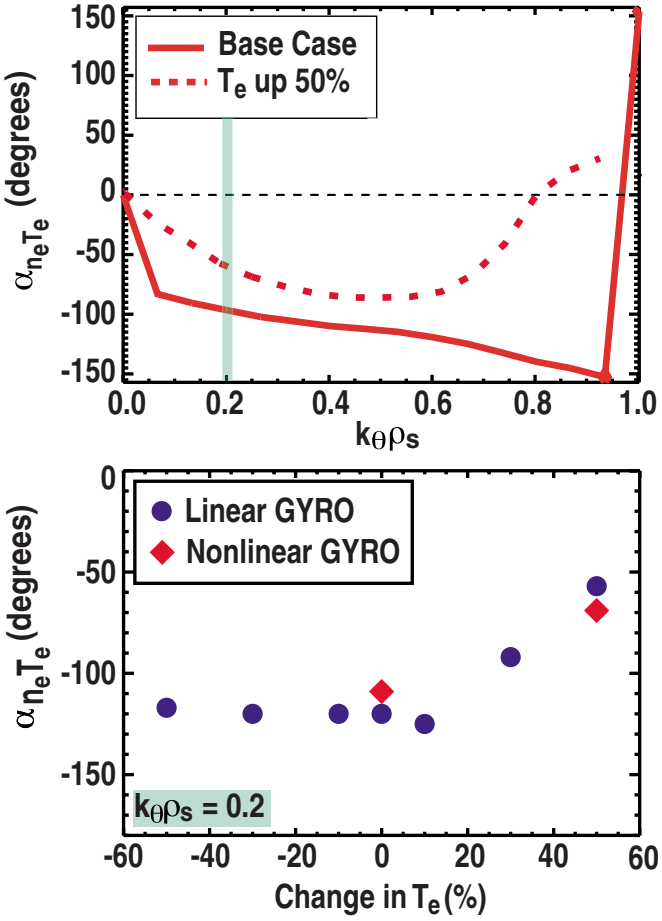

FIG. 1. (Color online) The wave number spectrum of $\alpha_{n_eT_e}$ at ρ=0.5 calculated from nonlinear GYRO simulations shows the decrease in cross phase as T_e is increased by 50%. Values of $\alpha_{n_eT_e}$ at $k_\theta\rho_s$=0.2 plotted vs percent change in T_e. Linear GYRO runs (blue circles) and nonlinear GYRO runs (red diamonds) show good agreement both for the magnitude of the cross-phase angle and the trend with increasing T_e.

that density and electron temperature fluctuations are out of phase, $\alpha_{n_eT_e}\approx-110°$.[9] Building on this result, a T_e scan was studied with GYRO to assess whether or not $\alpha_{n_eT_e}$ will change given an experimentally realizable change in plasma parameters. An experimental T_e scan is motivated by the availability of a high-power ECH system at DIII-D, which can be used to increase T_e in beam-heated L-mode plasmas by as much as 50% with little to no change in $1/L_{T_e}$. In these pre-experiment simulations, T_e and ∇T_e were increased up to 50% ($1/L_{Te}$ is constant). All other input parameters (such as n_e, T_i, and E_r) were held constant, but parameters directly dependent on T_e, e.g., collisionality and temperature ratio, were allowed to vary in the simulations as T_e is scanned. Table I compares the input parameters used for two pre-experiment GYRO simulations, corresponding to a "Base" case and a "High T_e" case.

The pre-experiment simulations show a significant decrease in $\alpha_{n_eT_e}$ at long wavelengths ($k_\theta\rho_s<0.5$) in the "High T_e" case. The predicted trend for $\alpha_{n_eT_e}$ at ρ=0.5 at the outboard midplane is shown as a function of normalized wave number in Fig. 1(a). The pre-experiment simulations predicted that $\tilde{n}_e$ and $\tilde{T}_e$ are out of phase, $\alpha_{n_eT_e}\approx-110°$, in ITG

TABLE II. Results from the pre-experiment set of local, nonlinear GYRO simulations comparing transport and turbulence at $\rho=0.5$ for the "Base" and "High T_e" cases. Statistical errors are 1% for turbulence levels and 2%–3% for transport levels.

Parameter	Base 128913	High T_e 128913	Change (%)
χ_{GB} (m^2/s)	0.866	1.590	+84
χ_e/χ_{GB}	2.67	3.62	+36
Q_e (MW)	0.96	3.60	+275
χ_i/χ_{GB}	5.15	5.71	+11
Q_i (MW)	1.06	2.16	+104
$e\tilde{\varphi}/T$ (%)	2.30	2.51	+8
$\tilde{n}_e/n_e$ (%)	1.08	1.00	−7
$\tilde{T}_e/T_e$ (%)	1.56	2.49	+60
$\tilde{T}_i/T_i$ (%)	1.56	1.30	−20
$\tilde{T}_e/T_e/\tilde{n}_e/n_e$	1.4	2.5	+128
$\alpha_{n_e\phi}(k_\theta\rho_s\approx0.2)$	−23°	−46°	+100
$\alpha_{T_e\phi}(k_\theta\rho_s\approx0.2)$	−138°	−138°	⋯
$\alpha_{n_eT_e}(k_\theta\rho_s\approx0.2)$	−109°	−69°	−36

dominant L-mode plasmas. The pre-experiment simulations also showed that $\alpha_{n_eT_e}$ decreased to $\alpha_{n_eT_e}\approx-70°$ when the electron temperature is increased by 50% ($1/L_{T_e}$ constant). In the nonlinear simulations, the change in cross-phase angle is accompanied by a change from ITG turbulence to TEM turbulence as T_e increases. For the "Base" and "High T_e" cases in the pre-experiment simulations, the linear cross-phase angle calculated with GYRO is in agreement with the nonlinear cross-phase angle, Fig. 1(b). Using this observation, a larger T_e scan is performed using linear GYRO simulations. The same trend in $\alpha_{n_eT_e}$ is observed. The agreement between the linear and nonlinear theory for the cross-phase angle in these cases is consistent with past results showing that for ITG and TEM turbulence with low turbulence drive (e.g., $a/L_T\leq3$) there is good agreement between nonlinear and linear cross-phase angles.[14]

Changes in turbulence characteristics (amplitudes and cross-phase angles) and thermal transport are output from the two nonlinear pre-experiment simulations and are summarized in Table II. The rms fluctuation levels from the pre-experiment simulations are taken at the midplane and averaged over the simulation box. These values do not include synthetic diagnostic modeling, which reduces the midplane fluctuation levels typically by a factor of 2 or more and also affects the shape of the frequency power spectra.[18] All fluctuation levels have standard deviations for the rms fluctuation level of approximately 1%. Note that in both the pre-experiment "Base" and "High T_e" cases the electrons do not follow a Boltzmann (adiabatic) response, the cross-phase angle between density and potential fluctuations is finite, $\alpha_{n_e\phi}\neq0$, and $e\tilde{\phi}/T\neq\tilde{n}_e/n_e$. This is expected because the finite electron transport in the simulations results from the nonadiabatic part of the distribution function. Interestingly, the change in $\alpha_{n_eT_e}$ predicted by the simulations is accompanied by a large factor of 2 change in cross-phase angle $\alpha_{n_e\phi}$, but there is no change in cross-phase angle between electron temperature and potential fluctuations, $\alpha_{T_e\phi}$. The large increases in electron heat transport in the simulation result both from the change in cross-phase angle $\alpha_{n_e\phi}$ and from the increase in electron temperature fluctuation amplitude. The increase in the cross-phase angle $\alpha_{n_e\phi}$ also contributes to the increase in particle transport even though a decrease in $\tilde{n}_e/n_e$ is predicted. The ion temperature fluctuation level, $\tilde{T}_i/T_i$, is predicted to decrease by 20%, although the ion thermal transport increases by 11% in the simulations.

These pre-experiment nonlinear GYRO simulations of beam-heated L-mode plasma conditions show that long-wavelength turbulence is changed from ITG-driven to TEM-driven in the cases with higher electron temperature. Extensive parameter scans for linear stability calculations using TGLF (Ref. 24) indicate that for typical beam-heated L-mode plasma parameters, these changes in turbulence drive are a result of decreases in collisionality and increases in T_e/T_i. The correlation between changes in $\alpha_{n_eT_e}$ and changes in ITG/TEM drive is of interest because theory suggest that the sign of $\alpha_{n_eT_e}$ could be used to identify the dominant instability driving the observed turbulence[13] in a manner similar to using measurements of the propagation direction of turbulence in the plasma frame to identify ion or electron drift wave type modes.[1,2]

III. COUPLED REFLECTOMETRY AND CECE DIAGNOSTICS

Experimentally the cross-phase angle between long wavelength density and electron temperature fluctuations, $\alpha_{n_eT_e}$, is measured locally in the core plasma using a V-band multichannel X-mode quadrature reflectometer and a W-band multichannel X-mode CECE diagnostic. The two fluctuation diagnostics are coupled together using a multiplexer so that the same antenna and plasma viewing optics can be used. The data from the CECE and reflectometer diagnostics are recorded on the same digitizer so that time bases for the $\tilde{n}_e$ and $\tilde{T}_e$ signals are identical. The CECE diagnostic (similar to that described in Ref. 7) is used to measure local, long-wavelength ($k_\theta\rho_s<0.3$) electron temperature fluctuations. The CECE system has two tunable, narrow-band ($\Delta f^{-3dB}\approx110-118$ MHz, with tunable central frequency range 6–17.6 GHz) channels which measure second harmonic electron cyclotron emission (ECE) in the range $88<f_{ECE}<95$ GHz ($B_T=2$ T) and two fixed frequency, narrow-band ($\Delta f^{-3dB}\approx100$ MHz) channels viewing $f_{ECE}=91.6$ GHz and $f_{ECE}=93.6$ GHz. The multichannel quadrature reflectometer diagnostic is used to measure local, long-wavelength ($k_\theta\rho_s<0.5$) density fluctuations. Full capabilities of this system are described in Ref. 11. For this experiment, the diagnostic is specifically configured so that the system operates as a quadrature reflectometer rather than as a Doppler backscattering system. For this experiment there were five launched frequencies, which were tunable on a shot-by-shot basis and scanned over the range $66<f_{launch}<73$ GHz, with a 250 MHz spacing between frequencies.

A diagram of the coupled CECE radiometer and reflectometer diagnostics at DIII-D is shown in Fig. 2. The shared plasma viewing optics localize the sample volumes toroi-

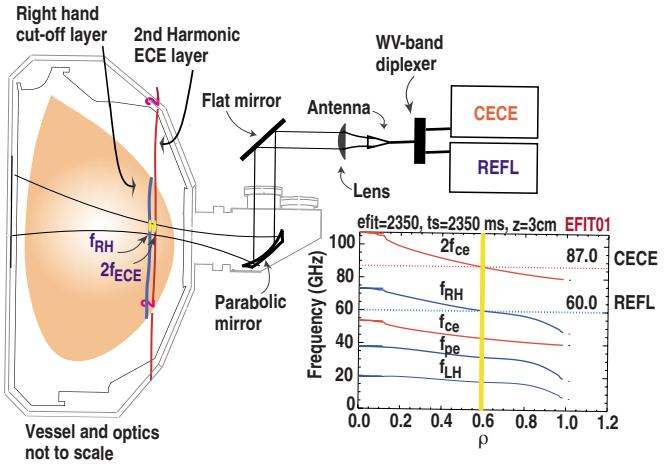

FIG. 2. (Color online) Diagram of coupled CECE and reflectometer diagnostics at DIII-D. The inset shows profiles of plasma frequencies with example values of $2f_{ce}$ and f_{RH} where CECE and reflectometer radial measurement locations will overlap.

dally and poloidally. Radial overlap is obtained because the X-mode correlation ECE radiometer measurement volume is radially localized to a narrow resonance layer for second harmonic ECE at $2f_{ce}$ in optically thick plasmas. The X-mode quadrature reflectometer measurement volume is localized to the region where the right-hand cutoff frequency, f_{RH}, matches the launch frequency, f_{launch}. The sample volumes for the CECE and reflectometer diagnostics are approximated by Gaussian profiles defined by the e^2-folding lengths in the vertical and radial directions. For the CECE measurement, the sample volume dimensions are approximately $\Delta z=3.2$ and $\Delta r\approx 1$ cm, determined by the measured antenna pattern and the width of the last emission layer, respectively. The sample volume dimensions of the reflectometer measurement are determined by a combination of antenna pattern, flux surface curvature, and refractive effects and are estimated to be $\Delta z\approx 3$ and $\Delta r\approx 1$ cm. The inset in Fig. 2 shows profiles of plasma frequencies with example values of $2f_{ce}$ and f_{RH} where CECE and reflectometer radial measurement locations will overlap. To measure correlation between the two fluctuating fields, the reflectometer and CECE measurement volumes need to be separated by less than the correlation length of the turbulence, which is measured to be 2–3 cm in the L-mode plasmas of interest described later in Sec. IV.

The correlation between a reflectometer signal and an ECE signal is calculated using standard Fourier transform analysis techniques.[25] The data series for the density fluctuations (reflectometer signal) and electron temperature fluctuations (ECE signal) from some long, stationary time period of interest are broken up into a reasonably large number, $n_d>1000$, of statistically independent records. Each record is Fourier transformed and the autospectrum function estimate, $|\langle S_{\tilde{n}_e}\rangle|^2$ and $|\langle S_{\tilde{T}_e}\rangle|^2$, and cross-spectrum estimate, $\langle S^*_{\tilde{n}_e} S_{\tilde{T}_e}\rangle$ are calculated as an ensemble average; the * indicates a complex conjugate. From these, the coherency, $\gamma_{n_eT_e}$, as a function of frequency between the density fluctuations and electron temperature fluctuations can be calculated as

$$\gamma_{n_eT_e}(f)=\frac{|\langle S^*_{\tilde{n}_e} S_{\tilde{T}_e}\rangle|}{|\langle S_{\tilde{n}_e}\rangle|^2|\langle S_{\tilde{T}_e}\rangle|^2}. \tag{2}$$

The cross-phase angle as a function of frequency between density and electron temperature fluctuations is defined as

$$tan[\alpha_{n_eT_e}(f)]=\frac{Im(\langle S^*_{\tilde{n}_e} S_{\tilde{T}_e}\rangle)}{Re(\langle S_{\tilde{n}_e} S_{\tilde{T}_e}\rangle)}. \tag{3}$$

From Ref. 25, the normalized random error in the coherency is defined as

$$\epsilon[\gamma_{n_eT_e}(f)]=\frac{\sqrt{2}(1-\gamma^2_{n_eT_e})}{|\gamma_{n_eT_e}|\sqrt{n_d}}, \tag{4}$$

and the standard deviation in the cross-phase angle is defined as

$$\text{s.d.}[\alpha_{n_eT_e}(f)]=\frac{(1-\gamma^2_{n_eT_e})^{1/2}}{|\gamma_{n_eT_e}|\sqrt{2n_d}}. \tag{5}$$

The expressions above are used to evaluate both experimental data and the output of nonlinear GYRO simulations. We also report frequency averaged phase angles with a variance and a standard deviation calculated using regular definitions.[25]

The reflectometer signals are detected in quadrature, which allows for both amplitude and phase information to be retained. From the quadrature system there are several reflectometer signals available: homodyne, $A(t)\cos\phi(t)$, complex amplitude, $A(t)e^{i\phi(t)}$, phase, $\phi(t)$, and amplitude, $A(t)$. The reflectometer phase signal, $\phi(t)$, should not be confused with the cross-phase angle of the turbulence, $\alpha_{n_eT_e}$. Measurements of density fluctuations with reflectometry are often difficult to interpret, and most theories of reflectometry consider only the reflectometer phase signal in order to extract information about the turbulent density fluctuations.[26] However, there is evidence that information about local, turbulent density fluctuations can be obtained from the reflectometer amplitude signal as well. Experimentally, it has been observed that the spectrum and fluctuation level of density fluctuations measured with the reflectometer amplitude and complex amplitude signals in tokamaks are in good agreement with measurements from Langmuir probes[27] and BES.[28] On the modeling side, recently a 2D full wave code was used to show that the amplitude signal, $A(t)$, reproduces most closely the true correlation length of density fluctuations in a regime characterized by low density fluctuation levels,[29] that is, when fluctuation levels are similar to those measured in the core plasma, $\delta n/n\sim 1\%$, rather than the edge plasma, $\delta n/n\sim 10\%$.

In this work, we have examined the correlation between an ECE radiometer signal and all available reflectometer signals. The highest coherency between $\tilde{n}_e$ and $\tilde{T}_e$ is found when using the reflectometer amplitude signal, $A(t)$. Figure 3 presents an example of correlated density and electron temperature fluctuations measured at DIII-D at $\rho\approx 0.6$ in an Ohmic plasma heated with ECH (no beams). The power spectrum of density fluctuations from the reflectometer amplitude signal

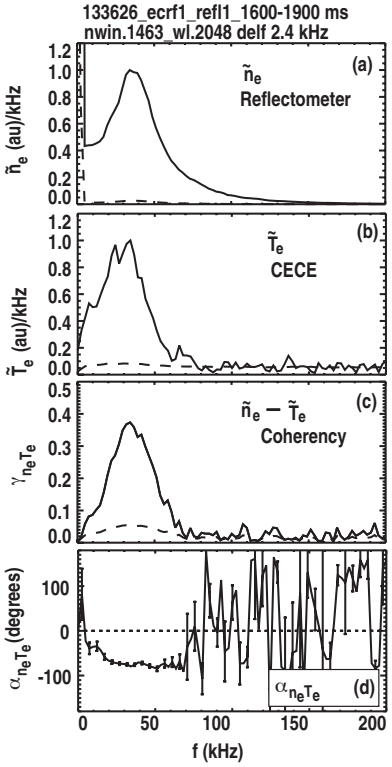

FIG. 3. Example of measured correlated long wavelength $\tilde{n}_e$ and $\tilde{T}_e$ in a plasma with only Ohmic heating and ECH (no beams) at DIII-D (133 626, $t=1600-1900$ ms, $\rho=0.6$). (a) The power spectrum of density fluctuations measured with the scattered power signal from the reflectometer, (b) the power spectrum of electron temperature fluctuations measured with CECE using a two-channel correlation technique, (c) the coherency spectrum of density and electron temperature fluctuations, and (d) the cross-phase angle spectrum between density and electron temperature fluctuations.

is shown in Fig. 3(a), the power spectrum of electron temperature fluctuations measured with CECE in Fig. 3(b), the measured coherency spectrum in Fig. 3(c), and cross-phase angle spectrum in Fig. 3(d). The power spectra are plotted versus frequency in kilohertz and normalized to the peak power in the frequency range $f>10$ kHz in order to compare the spectral shapes. In this plasma with only Ohmic heating and ECH, the turbulent $\tilde{n}_e$ and $\tilde{T}_e$ spectra are narrow in frequency due to small Doppler shifts of the turbulent spectrum in these low-rotation plasmas. Where strong coherency between the density and electron temperature fluctuations is observed, between 10 and 70 kHz, it is possible to clearly resolve the cross-phase angle, Fig. 3(d). Here the fields are roughly 60° out of phase. At higher frequencies where the fluctuations are no longer coherent, for example, above 70 kHz, $\alpha_{n_eT_e}$ is not resolved. The horizontal dashed lines in Figs. 3(a)–3(c) represent the statistical noise limit of the spectral estimates and are taken to be the standard deviation. In Fig. 3(d) the horizontal dashed line is drawn at $\alpha_{n_eT_e}=0$ for reference. Error bars plotted on the cross-phase angle represent the standard deviation calculated based on the coherency values and the number of records used in the ensemble average for the coherency and cross-power estimates.

When using the CECE system to measure electron temperature fluctuations, two channels that are incoherent with respect to intrinsic radiometer thermal noise, but coherent with respect to the turbulence fluctuations, need to be correlated using a two-channel correlation technique, $\langle S^*_{1,\mathrm{ECE}} S_{2,\mathrm{ECE}} \rangle$, to extract the spectrum and rms fluctuation level.[9,30–32] To correlate density and electron temperature fluctuations, we correlated a reflectometer signal with a single ECE signal. Sources of spurious correlations (e.g., due to electronic noise pick-up) between the two signals can be identified by correlating the signals in the absence of a plasma signal and can be eliminated. Since the reflectometer and CECE radiometer operate in different frequency ranges, any thermal noise present in the two systems will be uncorrelated and the thermal noise is expected to be small or zero for the reflectometer. Other unwanted but physically real correlations between the reflectometer and CECE signals can be present if the radiometer signal responds to density fluctuations. This can occur in two different cases. First, at high densities refractive effects become important as $2f_{ce} \sim f_{\mathrm{RH}}$ and the ECE radiometer signal becomes sensitive to $\tilde{n}$.[33] Second, because the optical depth for second harmonic EC emission scales as $\tau \propto n_e T_e$ and the emission intensity scales as $I \propto (1-e^{-\tau})$, density fluctuations can contribute to the measured fluctuating intensity at low densities when the optical depth is low, $\tau<3$.[32,33] In all the experimental results shown here the density is low enough that refractive effects are negligible and the density is high enough that $\tau>3$. Because of this, no contribution from density fluctuations to the ECE temperature fluctuation signal is expected.

IV. EXPERIMENTAL RESULTS

Experimentally we attempted to qualitatively test the pre-experiment predictions from GYRO, described in Sec. II, using quasistationary, sawtooth-free, beam-heated L-mode plasmas. The L-mode discharges have magnetic field $B_T=2.0$ T and plasma current $I_p=1$ MA. An upper single-null divertor plasma configuration is used with major radius, $R=1.63$ m, minor radius $a=0.62$ m, and elongation $\kappa=1.6$. This plasma configuration is chosen to avoid an L-H transition when strong auxiliary heating is applied. The experiments use deuterium neutral beam injection (NBI) in the cocurrent direction and ECH, with $P_{\mathrm{NBI+ECH}}>5$ MW. The beam heating began at $t=300$ ms to delay the onset of sawteeth beyond $t=1700$ ms by heating the electrons and increasing current diffusion time. A first discharge (reference shot 138 040) was heated with 2.5 MW of coinjected neutral beam power; no ECH was used. In the second discharge (reference shot 138 038), an additional 2.4 MW of ECH power (X-mode polarization) was launched from the low field side and deposited at the second harmonic ECE resonance layer at $\rho=0.4$. The time period of interest in both cases is the 250 ms quasisteady, sawtooth-free L-mode plasma between $t=1400-1650$ ms. During the time period of interest there is no evidence on magnetic signals or ECE signals of any large amplitude magnetohydrodynamic activity such as tearing modes. However, there is low level Alfvén eigenmode (AE) activity detected by the BES system inside of $\rho=0.4$. This is outside the measurement region for the

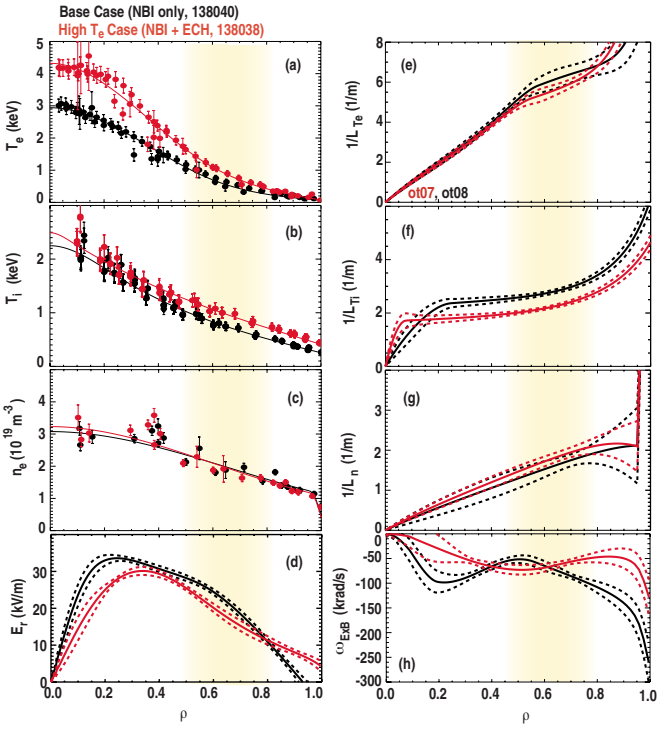

FIG. 4. (Color online) Measured plasma profiles comparing reference shots with NBI only (black) and a shot with NBI and ECH (red-grey), corresponding to a "Base" case and "High T_e" case, respectively. Data from 138 038 (red-grey) and 138 040 (black), $t=1525$ ms are shown.

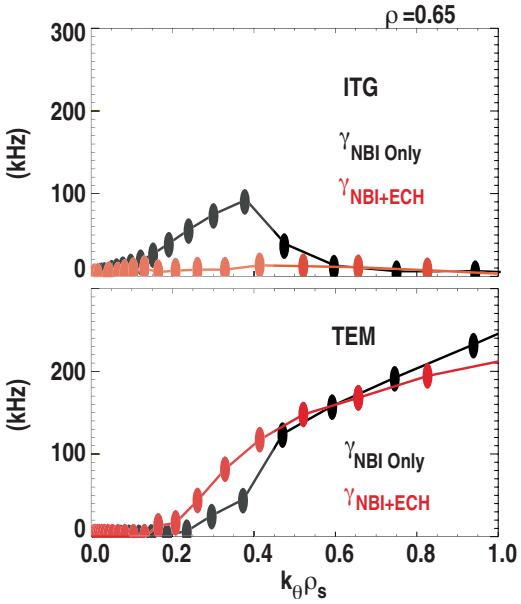

FIG. 5. (Color online) Changes in linear stability of the ITG mode and TEM calculated using TGLF comparing reference shots 138 040 and 138 038 corresponding to a "Base" case (black) and "High T_e" case (red-grey), respectively. Results at $\rho=0.65$ in 138 038 (red-grey) and 138 040 (black) at $t=1525$ ms are shown.

fluctuation diagnostics, and variations in density and temperature associated with these modes do not directly impact the turbulence measurements.

The time chosen for profile analysis and comparisons with GYRO simulations is $t=1525$ ms in the reference shots 138 038 and 138 040. Radial profiles of n_e were measured in the experiments using Thomson scattering[34] and CO_2 interferometers.[35] Electron temperature, T_e, profiles are measured by Thomson scattering and a 40 channel ECE radiometer[36] (this radiometer is independent of the CECE system). The profiles of ion temperature, T_i, and radial electric field, E_r, were measured by charge exchange recombination spectroscopy.[37] The measured experimental profiles at $t=1525$ ms for reference shots 138 038 (red-grey) and 138 040 (black) are shown in Fig. 4. With ECH, the electron temperature T_e and ∇T_e increased factors of 1.4 in the core and factors of 1.5–1.6 in the fluctuation measurement region near $\rho \approx 0.55$, 0.65, and 0.75 [Figs. 4(a) and 4(b)]. The ion temperature, T_i [Fig. 4(c)], increased in the measurement region due to increased collisional energy transfer between electrons and ions. The density profile [Fig. 4(e)] was matched in the two discharges using feedback control on the line averaged density and edge gas puff fueling. In Fig. 4, yellow shading indicates the radial region of interest for the turbulence measurements. Dashed lines indicate a one-sigma standard deviation due to random errors on the measurements. Dashed lines for statistical error bars are also shown on the gradient scale lengths and $E\times B$ shear derived from the spline fits to the measured profiles.

Overall, there was a decrease in collisionality, an increase in T_e/T_i, and an increase in the ratio of the gradient scale lengths, L_{T_i}/L_{T_e}, in the experiment. These changes will favor TEM drive relative to the ITG mode drive.[4,38] There is little to no change in the ion temperature gradient, ∇T_i, or the density gradient, ∇n, in the measurement region. During ECH there was very little change in $1/L_{T_e}$ [Fig. 4(b)] and $1/L_{n_e}$ [Fig. 4(f)] across the radial region of interest. However, there was a decrease in $1/L_{T_i}$ [Fig. 4(d)] at all radial locations due mainly to the increase in T_i of 30%. The effective charge state Z_{eff} increased across the radial range of interest from 1.9 to 2.5. Linear stability analysis of drift wave type instabilities was performed using the TGLF code[24] using local parameters taken from the measured profiles as input. TGLF does not evolve the linear gyrokinetic equation in time (initial value). Instead, TGLF solves a system of moment equations for the eigenvalues, which allows the calculated growth rate and real frequency wave number spectra for the ITG and TEM to be tracked independently. Linear stability analysis for the two reference shots shows that the increase in electron temperature resulted in an increase in the TEM growth rate at low-k and a decrease in the ITG-mode growth rate, consistent with expectations from the pre-experiment simulations. The results for $\rho=0.65$ are shown in Fig. 5 and are similar to results at $\rho=0.55$ and 0.75. In Fig. 5, yellow shading indicates the radial range of interest for the turbulence measurements.

The target conditions for this experiment were chosen in an attempt to minimize changes in $E\times B$ shear as T_e was increased. However, in the experiment we observed that the addition of ECH did change the radial electric field profile, resulting in a slight reduction in E_r [Fig. 4(g)]. There are also slight changes (just outside the statistical error bars) in the Hahm–Burrell shearing rate, $\omega_{E\times B}$, in the high T_e shot [Fig.

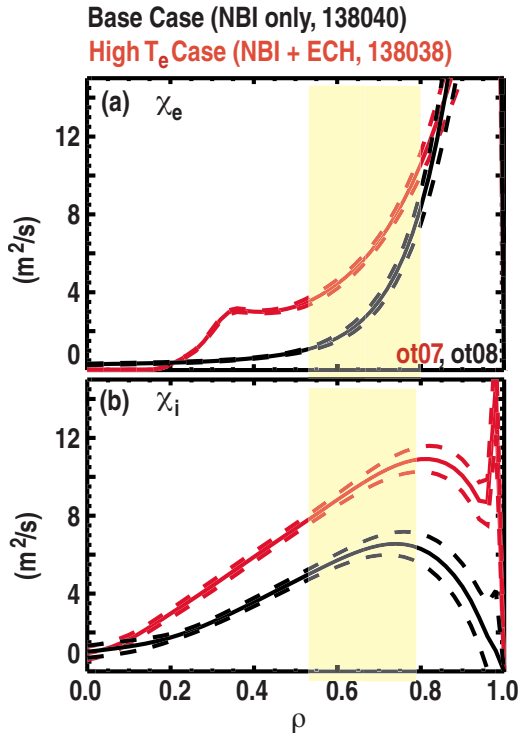

FIG. 6. (Color online) Changes in transport as calculated using ONETWO comparing a "Base" case (black) and a "High T_e" case (red-grey). Experimental profiles from reference shots 138 038 and 138 040 at $t=1525$ ms were used as input to ONETWO. Dashed lines indicate a one-sigma standard deviation resulting from random uncertainties in the input profiles.

4(h)], at $\rho=0.55$ and 0.65, but there is a significant reduction in $E\times B$ shear at $\rho=0.75$ when T_e was increased. Langmuir probe measurements in the edge of tokamak plasmas[39] and in basic plasma experiments[40] show that the $E\times B$ shear can strongly affect the cross-phase angle between fluctuating fields, and theory has shown that changes in the cross-phase angles due to $E\times B$ shear can impact transport more than changes in turbulence amplitudes.[41]

Power balance analysis is performed with the ONETWO code[42] using as input the experimentally measured profiles of density, n_e, from Thomson scattering[34] and CO_2 interferometers,[35] T_e from ECE radiometry[36] and Thomson scattering, ion temperature, T_i, and toroidal rotation, v_{rot}, from charge exchange recombination spectroscopy[37] and radiated power from bolometer arrays.[43] There were increases in thermal transport in the experimental "High T_e" case (138 038) compared to the "Base" case (138 040). Figure 6 shows the experimentally inferred electron and ion diffusivities, χ_e and χ_i, respectively, from the reference shots. To estimate uncertainties for the transport results, the n_e, T_e, T_i, and v_{rot} data from experimental profiles for the two reference shots are varied in a Monte Carlo analysis to produce a set of 100 spline fits to each profile. These 100 spline fits are used as input to ONETWO, which is run 100 times to produce an ensemble of transport results. The mean from this set of 100 ONETWO runs and the standard deviation of the mean are calculated. The mean thermal diffusivities are shown in Fig. 6 as solid lines and the standard deviation is shown as dashed lines. This is an estimate of the experimental uncertainty in the reported transport levels based on random errors in the measured density, temperature, and rotation profiles. Any effects due to potential systematic errors are not addressed by this estimate of the power balance uncertainties. In Fig. 6, yellow shading indicates the radial range of interest for the turbulence measurements.

The cross-phase angle between density and electron temperature fluctuations was measured using the coupled reflectometer-CECE system described in Sec. III. At the inner two core radial locations, $\rho=0.55$ and 0.65, we observed a decrease in $\alpha_{n_eT_e}$ consistent with the predicted trend. However, at $\rho=0.75$, there was no change in the cross-phase angle outside the error bars. Fluctuation data were averaged over the 250 ms quasisteady, sawtooth-free L-mode plasma between $t=1400-1650$ ms to improve the signal to noise ratio. The reference shots were repeated and the fluctuation diagnostics scanned on a shot by shot basis to measure turbulence at three different radial locations. On each shot, there are twenty reflectometer-CECE channel pairs from the multichannel diagnostics that are used to calculate the coherency and cross-phase angle between $\tilde{n}_e$ and $\tilde{T}_e$. In these L-mode plasmas with coinjected neutral beams, the turbulent $\tilde{n}_e$ and $\tilde{T}_e$ spectra and the cross-spectrum are broad in frequency due to large Doppler shifts caused by the $E\times B$ rotation, in contrast to the narrow spectra seen in Ohmic plasmas (e.g., Fig. 3). To compare changes in cross-phase angle between shots we selected only data with mean cross-phase angle in the frequency range $f=150-300$ kHz that had a variance of 20° or less. This is done to minimize changes in the cross-phase angle that may be due to shot-by-shot variations in sample volume separation. These effects are discussed in more detail in Sec. V. In Fig. 7 the measured coherency and cross-phase angle between density and electron temperature fluctuations is shown at $\rho=0.55$, 0.65, and 0.75. In all cases the cross-phase angle is found to be negative when taking the $\tilde{n}_e$ signal as the reference. In Fig. 7, results from discharges corresponding to the "Base" case with beam heating only are shown in black and the "High T_e" case with beam heating in addition to ECH is shown in red. Dashed lines in the coherency plots indicate the statistical noise floor and error bars on the cross-phase angle are calculated at each frequency based on the coherency level and the number of records in the ensemble average. The measured cross-phase angle at $\rho=0.55$ shows a decrease as T_e is increased. Shown in Figs. 7(a) and 7(b) the coherency at $\rho=0.55$ is nearly equal and the cross-phase angle has decreased from $\alpha_{n_eT_e}=-127°\pm17°$ to $\alpha_{n_eT_e}=-87°\pm8°$. The measured cross-phase angle at $\rho=0.65$ shows the clearest decrease with higher T_e. Shown in Figs. 7(c) and 7(d) the coherency at $\rho=0.65$ is nearly equal in both cases, but the measured cross-phase angle has decreased from $\alpha_{n_eT_e}=-110°\pm11°$ to $\alpha_{n_eT_e}=-61°\pm11°$. The measured cross-phase angle at $\rho=0.75$, in contrast to the two inner radii, showed no change in the cross-phase angle (outside error bars) in the shot with higher T_e. Here, shown in Figs. 7(e) and 7(f), the coherency is larger in the high T_e case and the measured cross-phase angle decreased from $\alpha_{n_eT_e}=-101°\pm8°$ to $\alpha_{n_eT_e}=-89°\pm8°$ at $\rho=0.75$. We note that at this outermost

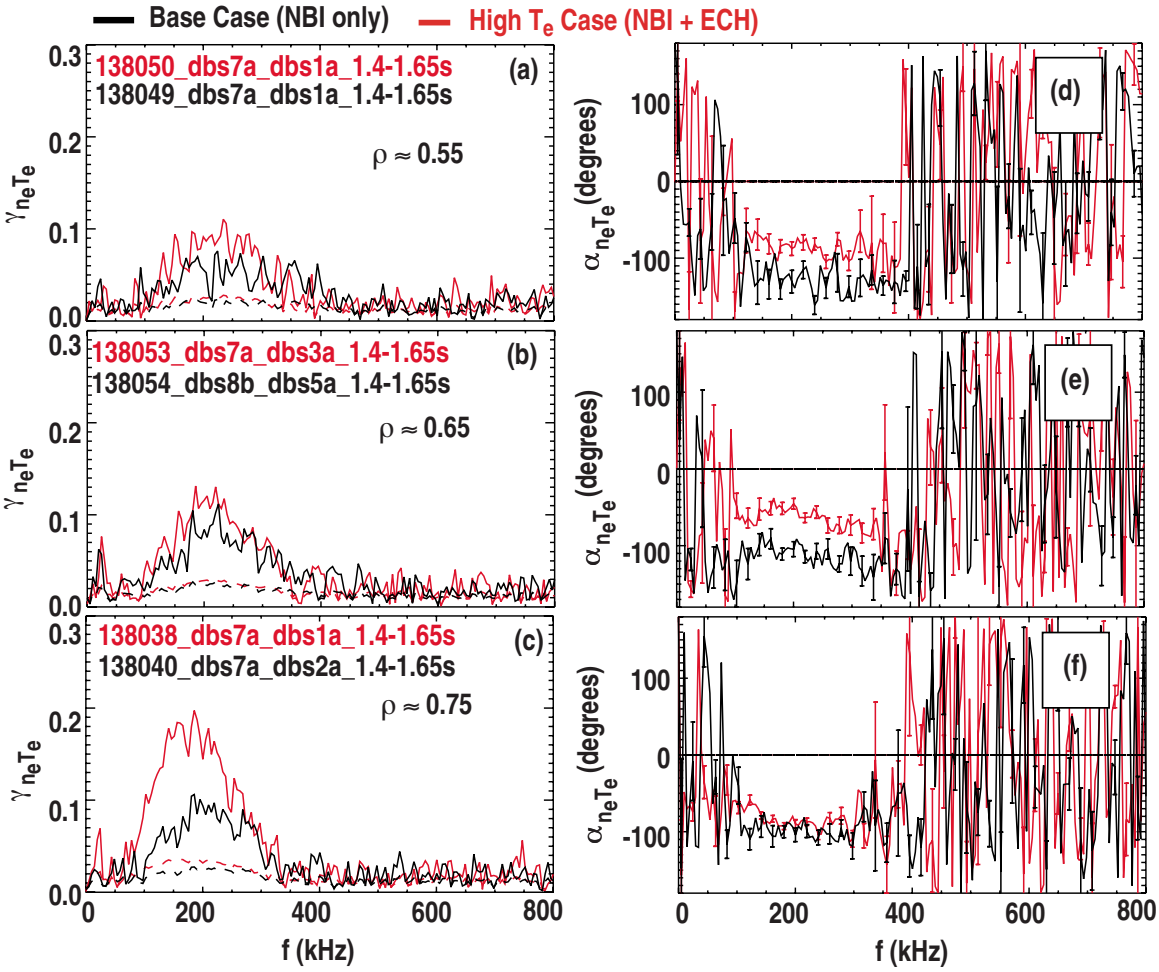

FIG. 7. (Color online) The measured coherency, $\gamma_{n_eT_e}$, and cross-phase angle, $\alpha_{n_eT_e}$, comparing "Base" cases (black) and "High T_e" cases (red-grey) are shown at three radial locations. At ρ=0.55 and 0.65 smaller cross-phase angles are measured in the High T_e Case. At ρ=0.75 there is no change in cross-phase angle outside experimental error bars. Horizontal dashed lines on the coherency plot indicates a statistical noise limit, error bars on the cross-phase angle are the one-sigma standard deviations, and a horizontal line at $\alpha_{n_eT_e}$=0 is plotted for reference.

measurement location, ρ=0.75, the plasma is optically thick with optical depth, τ>3. The radial profile of the $\alpha_{n_eT_e}$ is shown in Fig. 8. The plotted values are the average cross-phase angle in the frequency range 150–300 kHz, the errors bars are the standard deviation. In the "Base" case (black), the experimental results show that $\alpha_{n_eT_e}$ decreases as radius increases, but in the "High-T_e" case (red-grey), the smallest cross-phase angle between the two fields is measured at ρ=0.65.

Experimentally we observed that when two radially separated CECE signals are cross correlated, the cross-phase angle between them is zero and the coherency decays as the channel separation is increased. This is also true for radially separated reflectometer signals. The decay in coherency between radially separated turbulence measurements is used for measurements of the radial correlation length of the turbulence.[8] This analysis method is general and can be done using signals from CECE, reflectometry, BES, or Langmuir probe diagnostics. Changes in coherency between the $\tilde{n}_e$ and $\tilde{T}_e$ on a shot-by-shot basis was observed and is believed to be dominated by variations in the spatial separation of the reflectometer and CECE sample volumes. In general, the

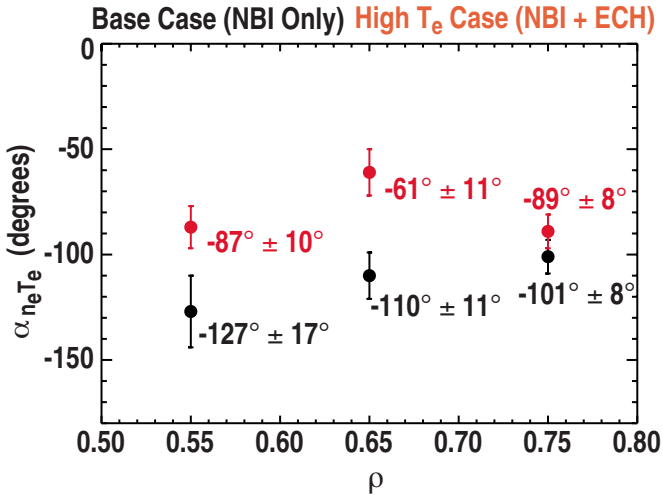

FIG. 8. (Color online) The "Base" case (black) and the "High-T_e" case (red-grey) cross-phase angles measured at three radial locations. The plotted values are the average cross-phase angle in the frequency range f =150–300 kHz, the errors bars are the one-sigma standard deviation on the frequency averaged cross-phase angle.

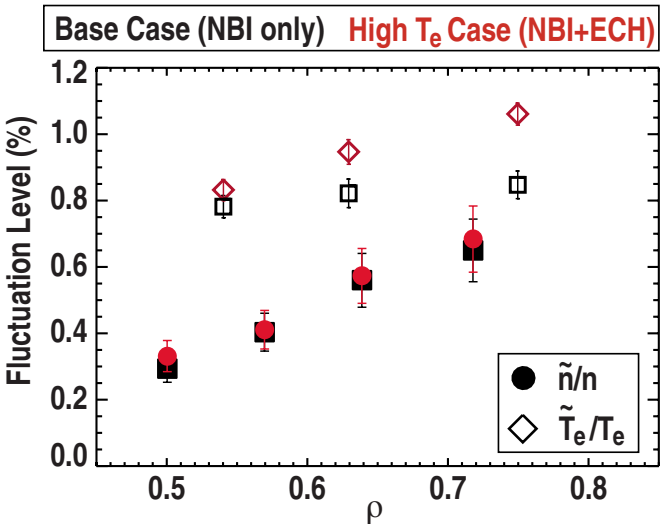

FIG. 9. (Color online) The measured changes in long wavelength electron temperature and density fluctuation levels measured with CECE and BES, respectively. The electron temperature fluctuation level is obtained by integrating the CECE cross-power spectrum between $f=30-240$ kHz and long-wavelength density fluctuation level is obtained by integrating the BES cross-power spectrum between $f=70-500$ kHz. Error bars represent the experimental uncertainty in the measurements.

TABLE III. Local parameters at $\rho=0.65$ from reference discharges 138 040 and 138 038 at $t=1525$ ms, corresponding to an experimental "Base" case and "High T_e" case, respectively. These are used as inputs for the postexperiment GYRO simulations.

Parameter	138040 "Base" case	138038 "High T_e"	Change (%)
ρ	0.65	0.65	···
a (m)	0.62	0.62	···
c_s/a (kHz)	260	330	+27
n_e (10^{19} m^{-3})	1.96	1.94	···
T_i (keV)	0.736	0.967	+31
T_e (keV)	0.538	0.871	+62
a/L_{n_e}	1.34	1.50	···
a/L_{T_i}	2.31	1.85	−20
a/L_{T_e}	5.04	4.60	···
γ_{ExB} (c_s/a)	0.117	0.071	−40
ν_{ei} (c_s/a)	0.349	0.138	−60
T_i/T_e	1.367	1.110	−19
ρ^*	0.0018	0.0022	+22
Z_{eff}	1.928	2.646	+37
q	2.479	2.459	···
$\hat{s}$	1.506	1.508	···

sample volumes can be separated both radially and poloidally and the correlation between the two fields will be limited by the smallest correlation length, since it is not necessary that the correlation lengths of the electron and density fluctuations be the same or that radial and poloidal correlation lengths of one field be the same. Measurements of the radial correlation length of long wavelength density fluctuations are made in these plasmas using BES and the measured radial correlation length of long wavelength density fluctuations was $L_{\text{rad}}\approx 2.9$ cm in this case. Experimentally we observed that when the reflectometer and CECE signals are separated radially by $dr>2$ cm, the cross-phase angle can no longer be resolved.

Using the BES and CECE diagnostics in this experiment, we measured the relative density, $\tilde{n}/n$ and electron temperature fluctuation, $\tilde{T}_e/T_e$ levels in the core plasma. The measured changes in the electron temperature fluctuation level (obtained by integrating the CECE cross-power spectrum between 30–240 kHz) and long-wavelength density fluctuation level (obtained by integrating the BES cross-power spectrum between 70–500 kHz) for the two experimental conditions are shown in Fig. 9. Long wavelength $\tilde{T}_e/T_e$ increases during ECH, with larger increases at larger values of ρ. The measured long wavelength $\tilde{n}/n$ stays nearly the same at all radial locations measured. The ratio of the two-field fluctuation level, $(\tilde{T}_e/T_e)/(\tilde{n}/n)$ increases roughly 20% at $\rho=0.65$ and $\rho=0.75$, with little to no increase at $\rho=0.55$. Similar to the predictions, long wavelength $\tilde{T}_e/T_e$ increases, but the largest increase is at $\rho=0.75$, with little to no increase observed at $\rho=0.55$. In disagreement with predictions, the measured long wavelength $\tilde{n}/n$, stays roughly the same and does not decrease. However, due to increases in $\tilde{T}_e/T_e$, there is an increase in the ratio $(\tilde{T}_e/T_e)/(\tilde{n}/n)$ similar to predictions. High-k ($k_r\approx 35$ cm^{-1}) density fluctuations are monitored in the experiment using a backscattering diagnostic.[44] The high-k density fluctuations exhibited increases in measured $\tilde{n}$ of 6% in the High T_e Case. No measurements of $\tilde{T}_i/T_i$ are available, nor of cross-phase angles $\alpha_{n_e\phi}$ or $\alpha_{T_i\phi}$. The pre-experiment simulations did not include high enough wave numbers to furnish predictions that could be compared with experimentally measured intermediate-k and high-k turbulence.

V. INITIAL POSTEXPERIMENT GYRO SIMULATIONS

Nonlinear postexperiment GYRO runs for both experimental conditions ("Base" and "High T_e" cases) and at all three radial locations are in progress. Here we report only on results at $\rho=0.65$. The inputs for postexperimental GYRO simulations taken from the measured profiles for the two reference discharges are summarized in Table III.

The simulations for 138 038, the "High T_e" case, were run with a radial box size of $108\rho_s$ and radial grid resolution of $\Delta x/\rho_s<0.35$ in all cases. The simulations used 20 toroidal modes with separation $\Delta n=8$, which gives toroidal mode numbers n ranging from 0 to 152. This corresponds to a simulated wave number range of $k_\theta\rho_s=[0,1.2]$. The integration time step was $\tau=0.01a/c_s$. Time traces of the box-averaged ion and electron diffusivities for discharge 138 038 show that the transport has reached a steady, saturated state by $\tau=50a/c_s$ and time averaged simulation data over the range $\tau=[140-280]a/c_s$ are used for comparisons with experimental data. The statistical uncertainty in the GYRO calculated flows is estimated as the standard deviation over the simulation time interval of interest. Spectral densities for the ion and energy diffusion show that the ion energy diffusivity is well resolved by this simulation at long wavelengths, but

TABLE IV. Postexperiment GYRO simulations from 138 038, $\rho=0.65$, $t=1525$ ms. Turbulence amplitudes and cross phase are compared with synthetic diagnostic results.

Parameter	GYRO	Experiment
Q_e (MW)	3.77 ± 0.06	2.43 ± 0.02
Q_i (MW)	0.34 ± 0.01	1.32 ± 0.02
$\tilde{T}_e/T_e$ (%)	1.07 ± 0.10	0.95 ± 0.05
$\tilde{n}/n$ (%)	0.25 ± 0.01	0.57 ± 0.06
$\alpha_{n_eT_e}$ (degrees)	71 ± 1	61 ± 12

the electron energy diffusion is less so, showing that contributions from $k_\theta\rho_s>1.0$ amount to 12% of the total flux. Simulations run with higher wave numbers included ($k_\theta\rho_s$ up to 2.0) show little change in the net energy flow for these parameters; however, more detailed box-size scans will be performed in the future to evaluate the effects of resolving higher-k modes in detail. For this case at $\rho=0.65$ from 138 038, the frequency-mode number spectra from the nonlinear GYRO simulations show that the potential fluctuations, electron density fluctuations, and electron temperature fluctuations all exhibit frequency responses consistent with predominantly TEM driven turbulence.

The experimental power flows taken from the ONETWO power balance analysis are compared with GYRO results for 138 038 in Table IV. Comparisons between the flows calculated by GYRO and the experimental flows show that the ion power flow is underestimated by nearly a factor of 3 and the electron power flows are overestimated by 50%. The experimental electron and ion power flow values are $Q_e=2.43\pm0.02$ MW and $Q_i=1.32\pm0.02$ MW, respectively. The GYRO calculated electron and ion power flow values are $Q_e=3.77\pm0.06$ MW and $Q_i=0.34\pm0.01$ MW, respectively. Error bars on the experimental power flows are estimated using a Monte Carlo analysis (as described in Sec. III) and error bars on the GYRO results are estimated from the statistical uncertainty in the simulations.[18] There are also disagreements between ONETWO results and the GYRO calculated particle transport: however, particle sources due to wall recycling are not well known and a detailed comparison with particle transport is not performed at this time. Power flows instead of diffusivities are compared to minimize the effect of uncertainties in the measured profile gradients.[18]

Along with the power flow comparisons, Table IV lists comparisons between GYRO synthetic diagnostic turbulence results and the experimental measurements. Synthetic BES and CECE diagnostics are applied to the GYRO results following the methods of Ref. 18. Using the synthetic diagnostics we find that the density fluctuation level predicted by GYRO underestimates BES measurements at this location by an amount outside the experimental error bars, but the predicted electron temperature fluctuation level is in agreement to within error bars with the CECE measurements. The experimental density and electron temperature fluctuation levels are $\tilde{n}/n=0.57\pm0.06\%$ and $\tilde{T}_e/T_e=0.95\pm0.05\%$, respectively. The GYRO calculated (with synthetic diagnostics) density and electron temperature fluctuation levels are $\tilde{n}/n=0.25\pm0.01\%$ and $\tilde{T}_e/T_e=1.07\pm0.10\%$, respectively. Similar to past simulations when electron heat flux did not match the experiment [Fig. 10 of Ref. 9] we find that the shape of the power spectra calculated from the GYRO synthetic BES and CECE signals does not agree with the measured power spectral shapes at low frequencies.

Using the GYRO results from the postexperiment simulation of shot 138 038 at $\rho=0.65$ to model the cross-phase angle measurements, we produced synthetic density and electron temperature fluctuation signals and analyzed them the same way as the experimental data. The sample volumes for the CECE and reflectometer diagnostics are approximated by Gaussian profiles defined by the e^2-folding lengths in the vertical and radial directions. For the CECE measurement, the sample volume dimensions are approximately $\Delta z=3.2$ cm and $\Delta r\approx1$ cm, determined by the measured antenna pattern and the width of the last emission layer. The sample volume dimensions of the reflectometer measurement are determined by a combination of antenna pattern, flux surface curvature, and refractive effects. They are estimated to be $\Delta z\approx3$ cm and $\Delta r\approx1$ cm. For this particular radial location, $\rho=0.65$, the centers of the sample volumes for the CECE and reflectometer are radially and poloidally displaced by $dr=R_{\mathrm{cece}}-R_{\mathrm{refl}}=0.5$ cm and $dz=z_{\mathrm{cece}}-z_{\mathrm{refl}}=0.3$ cm, respectively. This sample volume separation is calculated using the GENRAY ray tracing code[45] taking experimental profiles and equilibrium reconstruction into account. The experimental cross-power spectrum (normalized to compare spectral shape) and the cross-phase angle are compared with unfiltered GYRO results as well as the synthetic diagnostic results. Shown in Fig. 10(a) are the GYRO unfiltered (black-solid), synthetic diagnostic (blue-dashed), and experimental (red-grey) cross-power spectra. The use of the synthetic diagnostic spatial filter modifies the shape of the cross-power spectrum between $\tilde{n}_e$ and $\tilde{T}_e$, as seen in Fig. 10(a). The spatial filtering results in a reduction of power at higher frequencies. This effect is also observed when applying synthetic BES or CECE diagnostics to GYRO output: higher frequencies are filtered out and the fluctuation amplitude decreases.[18] The sensitivity of the cross-power spectrum to details of the sample volume size is to be contrasted with the robustness of the cross-phase angle, which is largely unaffected by the sample volume size. As shown in Fig. 10(b) the sign and magnitude of the cross-phase angle are not affected by the spatial filtering, except at higher frequencies where the signal levels are significantly attenuated by the spatial filtering. Both with and without the spatial filtering applied there is good quantitative agreement between the experiment and the simulation for the average cross phase between 150–300 kHz, with GYRO cross-phase angle $\alpha_{n_eT_e}=-71^\circ\pm1^\circ$, and experimental cross-phase angle $\alpha_{n_eT_e}=-61^\circ\pm12^\circ$. Note that the experimental phase angle is meaningfully compared with simulations only where it is resolved (frequencies where the coherency is high). Outside the frequency range $90<f<350$ kHz the measured $\alpha_{n_eT_e}$ is in the noise. The error bars on the experimental and the GYRO calculated cross-phase angles are from statistical considerations only, where the

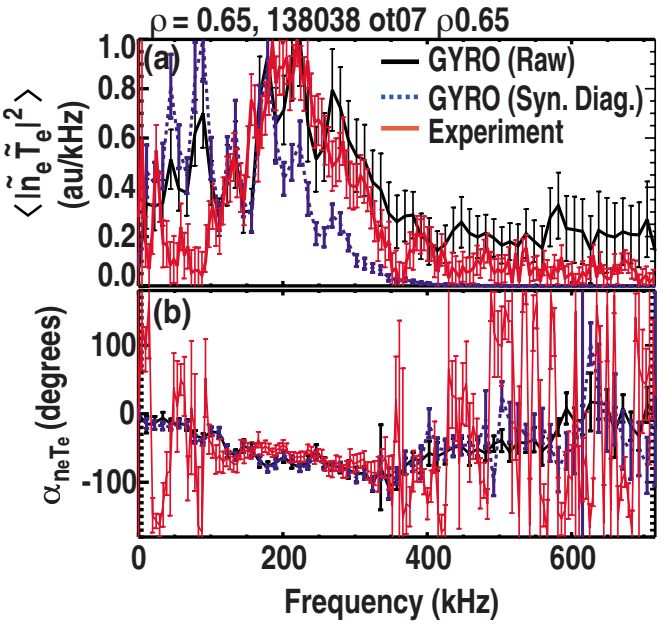

FIG. 10. (Color online) Comparison of experimental results at $\rho=0.65$ to postexperimental simulation results using the local parameters from 138 038, $t=1525$ ms as input. (a) The GYRO unfiltered (black-solid), synthetic diagnostic (blue-dashed), and experimental (red-grey) cross-power spectra have been normalized to compare the spectral shape. (b) The GYRO unfiltered (black-solid), synthetic diagnostic (blue-dashed), and experimental cross-phase angles (red-grey) are compared. The one-sigma standard deviations are plotted as error bars at each frequency in (a) and (b). Note that the experimental phase angle is meaningfully compared with the simulations only where it is resolved (frequencies where the coherency is high), between $90<f<350$ kHz. Outside this frequency range the measured $\alpha_{n_eT_e}$ is in the noise.

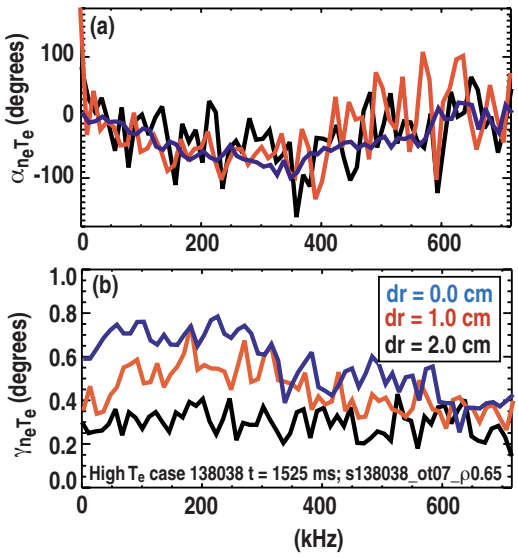

FIG. 11. (Color online) The sample volumes for the synthetic CECE and reflectometer signals are separated by $\Delta Z=z_{cece}-z_{refl}=0.3$ cm and the radial separation, dr, is scanned. The cross-phase angle is shown in (a) and the coherency is shown (b).

standard deviation of the cross-phase angle depends on the coherency and the number of records used in the ensemble average, Eq. (5). At fixed sample volume separation we varied the size of the sample volume (the $1/e^2$ power diameter of the Gaussian), to examine the resulting changes in coherency and the variance of the cross-phase angle. We found that 50% changes in the sample volume size led to 20% changes in the mean cross-phase angle.

In plasma turbulence measurements, poloidal separation of sample volumes leads to dispersion in the measured cross-phase angle spectrum due to poloidal propagation of the turbulence eddies in the background $E\times B$ flow. This effect has been observed at DIII-D with the coupled reflectometer and CECE measurements and is similar to dispersion seen in Langmuir probe measurements and BES measurements of plasma turbulence. In comparing shots with and without ECH to determine what, if any, changes in $\alpha_{n_eT_e}$ occur, cross-phase spectra with similar levels of dispersion are compared so that a change in reported cross-phase angle is not attributed to variations due to sample volume and channel separation effects. Radial separation of the reflectometer and CECE signals leads to reductions in the coherency and an increase in the variance of the average cross-phase angle. Due to these effects, there are experimental uncertainties associated with the mapping of the separation between reflectometer and ECE radiometer measurements in real space due to uncertainties in the experimentally measured density profile that is used in the ray-tracing analysis. To estimate the effects of sample volume separation, we varied the radial and poloidal separation of the sample volumes in the GYRO simulations about the experimentally estimated values. Examples of the sample volume separation sensitivity scans are shown in Figs. 11 and 12. In Fig. 11, the sample volumes for the synthetic CECE and reflectometer signals are separated by $\Delta Z=z_{cece}-z_{refl}=0.3$ cm and the radial separation, dr, is scanned. The changes in the cross-phase angle and the coherency due to the dr scan are shown in Figs. 11(a) and 11(b), respectively. Radial separation reduced the coherency, but left the cross-phase angle unchanged; although it did

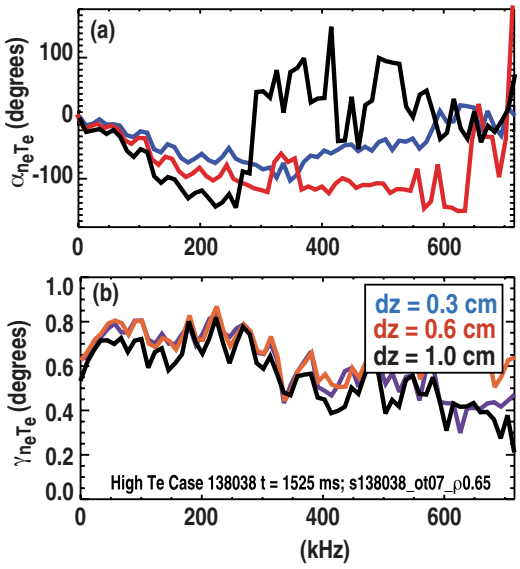

FIG. 12. (Color online) The sample volumes for the synthetic CECE and reflectometer signals are separated by $\Delta R=r_{cece}-r_{refl}=0.5$ cm and the vertical separation, dz, is scanned. The cross-phase angle is shown in (a) and the coherency is shown in (b).

increase the variance of the cross-phase as the coherency is reduced. In Fig. 12, the sample volumes for the synthetic CECE and reflectometer signals are separated by $\Delta R = r_{cece} - r_{refl} = 0.5$ cm and the vertical separation, dz, is scanned. The changes in the cross-phase angle and the coherency due to the dz scan are shown in Figs. 12(a) and 12(b), respectively. Changes in vertical separation leave the coherency unchanged but significantly alter the reported frequency averaged cross-phase angle. These sensitivity scans with the synthetic diagnostics show poloidal separation that produces dispersion in the cross-phase angle which will lead to an overestimate of the phase difference (frequency averaged). In contrast, radial separation does not change the average cross-phase angle, but it does significantly increase the variance.

The goal for this work was to compare the experimental "High T_e" and "Base" cases, but at this point in time no simulations for the base case reference discharge (138 040) have been completed with satisfactory results. Using the local experimental parameters from the reference discharge 138 040 at $t=1525$ ms as input to the codes, a saturated steady-state flux is obtained; however, the fluxes saturate at unrealistically low levels (e.g., $Q_e \sim 0.1$ MW) and the fluctuation intensity is condensed always in the highest wave number resolved in the simulation for both ion and electron energy diffusion. This issue has not been resolved by scanning the box size, radial resolution, range of mode numbers resolved, or by increasing the highest wave number simulated up to $k_\theta \rho_s = 3.0$. It is also not resolved by using an electrostatic simulation instead of an electromagnetic simulation, by removing the dynamic carbon, or by otherwise simplifying the simulation parameters. A "two-step" process to include the $E \times B$ shear was used.[18] When the simulation is run with the $E \times B$ shear off and with an increased turbulence drive (∇T_i increased by 10%) the result is a well-converged case where the turbulence is predominantly ITG and there is one primary mode driven strongly in the simulation, at $k_\theta \rho_s = 0.3$. However, at the second step in the "two-step" process with $E \times B$ shear turned back on, the simulation encounters the same issues as before and the fluctuation intensity is condensed at the highest wave number resolved in the simulation. This type of response in the simulations may indicate that a fully coupled ITG-TEM-ETG simulation[46] is needed to properly resolve the turbulence in this experimental case (138 040).

VI. SUMMARY OF RESULTS AND DIRECTIONS FOR FUTURE WORK

We have presented new measurements of the cross-phase angle, $\alpha_{n_e T_e}$, between long-wavelength ($k_\theta \rho_s < 0.5$) density, $\tilde{n}_e$, and electron temperature, $\tilde{T}_e$, fluctuations in the core ($0.5 < \rho < 0.8$) of the DIII-D tokamak.[6] The coherency and cross-phase angle between density and electron temperature fluctuations are measured by correlating a reflectometer amplitude signal and an ECE radiometer signal. The gyrokinetic turbulence simulation code GYRO is used to perform T_e scans prior to the experiment to predict a trend in $\alpha_{n_e T_e}$ that is qualitatively tested against experiment. The simulations predict that $\tilde{n}_e$ and $\tilde{T}_e$ are out of phase, $\alpha_{n_e T_e} \approx 110°$, in ITG dominant L-mode plasmas. The pre-experiment simulations showed that the cross-phase angle between $\tilde{n}_e$ and $\tilde{T}_e$ is expected to decrease to $\alpha_{n_e T_e} \approx 70°$ (as $\tilde{n}_e$ and $\tilde{T}_e$ become more in phase with each other) when the electron temperature is increased by 50%, with a/L_{T_e} held constant. The nonlinear simulation results and linear stability analysis show that TEM turbulence dynamics become increasingly important as T_e is increased. Neutral beam-heated L-mode tokamak plasmas were used to qualitatively test the predicted trend in $\alpha_{n_e T_e}$. Experimentally, the electron temperature, T_e, was increased 50% using local ECH in coinjected beam-heated L-mode plasmas. At all radii, the measurements show that in beam-heated plasmas (no ECH) density and electron temperature fluctuations are out of phase, with measured cross-phase angles qualitatively consistent with GYRO pre-experiment predictions. The measured magnitude of the cross-phase angle decreases significantly by approximately 45° at $\rho = 0.55$ and $\rho = 0.65$ in the High T_e discharges with NBI and ECH, consistent with expectations base on the pre-experiment simulations, but at $\rho = 0.75$ there is no change outside experimental uncertainty.

Linear stability analysis of the experimental reference shots shows that at all radii of interest the increase in electron temperature resulted in an increase in the TEM growth rate at low-k and a decrease in the ITG-mode growth rate, consistent with expectations from the pre-experiment simulations. This linear result and the pre-experiment nonlinear simulations suggest that changes in turbulence drive from dominantly ITG-mode to TEM is a possible explanation for the change in $\alpha_{n_e T_e}$ at $\rho = 0.55$ and $\rho = 0.65$. However, since significant changes in the cross-phase angle were only observed at two radii but linear stability analysis showed an increase in the TEM growth rate at low-k and a decrease in the ITG-mode growth rate at all radii, this explanation does not describe the response of the cross-phase angle at $\rho = 0.75$. This might be resolved by nonlinear simulations at this radius, to determine if the change in the ITG and TEM linear growth rates carries over into the nonlinear turbulence dynamics. Note that the pre-experiment simulations did not include changes in local input parameters consistent with experimentally observed increases in T_i, L_{T_i}, and Z_{eff}, or the decreases in $\omega_{E \times B}$. In the experiment, at all radii, the normalized density and temperature gradient scale lengths are 30%–90% larger than those used in the pre-experiment simulations. Another factor to consider at $\rho = 0.75$ is that there was a 60% reduction in the $E \times B$ shear at this radius. This parameter is expected to strongly affect the cross-phase angle.[41] This motivates experiments to isolate the effects of $E \times B$ shear on $\alpha_{n_e T_e}$.

In order to better understand the reasons for the good qualitative agreement with predictions at $\rho = 0.65$, but not at $\rho = 0.75$, quantitative comparisons between the measured $\alpha_{n_e T_e}$ and postexperiment nonlinear turbulence simulations are needed. The goal for this work was therefore to compare the experimental "High T_e" and "Base" cases quantitatively against traditional postexperiment simulations[18–20] at all radial locations, but at this point in time only simulations for the "High T_e" case reference discharge (138 038) at one ra-

dius have been completed with satisfactory results. The results from nonlinear postexperiment GYRO runs for shot 138 038 at $\rho=0.65$, $t=1525$ ms, have been compared to experimental power flows and measured turbulence characteristics. We found that for this case the GYRO predicted ion power flow underestimated the experimental value by nearly a factor of 3 and the electron power flows are overestimated by 50%. To compare with the turbulence quantities, synthetic diagnostics[18,22] were used. Synthetic reflectometer and CECE signals are generated from the GYRO output and are analyzed the same way as the experimental data. The synthetic diagnostic modeling shows that spectral shape of the density-electron temperature fluctuation cross-power spectrum is sensitive to the details of the sample volume size, consistent with expectations.[18] In contrast, the cross-phase angle is largely unaffected by the sample volume size. The cross-phase angle from the postexperiment simulations is in good quantitative agreement with the measured $\alpha_{n_eT_e}$ at $\rho=0.65$ in the experimental "High T_e" case (138 038, $t=1525$ ms). Experimentally we found $\alpha_{n_eT_e}=61^\circ\pm12^\circ$ and from GYRO $\alpha_{n_eT_e}=71^\circ\pm1^\circ$. We also found that the density fluctuation level predicted by GYRO underestimates BES measurements at $\rho=0.65$ by an amount outside the experimental error bars, but the predicted electron temperature fluctuation level is in agreement to within error bars with the CECE measurements. Similar to past simulations when electron heat flux did not match the experiment[18] we find that the shape of the power spectra from calculated from the GYRO synthetic BES and CECE signals does not agree with the measured power spectral shapes at the lowest frequencies.

The different levels of agreement found between the postexperiment GYRO results and experimentally measured two-field fluctuation levels, a cross-phase angle and power flows highlight the necessity of making multilevel comparisons at multiple radial locations and in multiple conditions. It is not clear how the different levels of agreement and disagreement between experiment and simulations among these different parameters should be assigned importance. Taking some guidance from an example of a "primacy hierarchy"[17] for validation discussed by Ref. 18, one could argue that the comparisons with the cross-phase angle and fluctuation levels are more important than the comparison with the transport fluxes because the turbulence quantities are more fundamental. However, uncertainties associated with application of the synthetic diagnostic models need to be evaluated carefully and compared against uncertainties in the transport analysis. Sensitivity scans for the synthetic diagnostics in this work showed that the GYRO predicted cross-phase angle is more sensitive to uncertainties in the spatial separation between the synthetic sample volumes than uncertainties in the sample volume size. The synthetic diagnostic sensitivity scans indicate that quantifying the uncertainty on the spatial separation used to reconstruct the synthetic reflectometer and CECE diagnostics is essential for evaluating the quality of the comparisons between GYRO results and experiments. Uncertainties in the location of the reflectometer measurement are due mostly to uncertainties in the measured density profile used as input for ray-tracing analysis. The same set of Monte Carlo generated density profile fits used to estimate errors on ONETWO results (Sec. III) will be used as input to the GENRAY code in the future to aid in assessing these uncertainties.

In these comparisons between experiment and GYRO simulations we used local experimental parameters as input. It is usually possible to improve the quantitative agreement in a single quantity at a single radial location by varying the input gradients within experimental error bars, and even to achieve better agreement with multiple quantities via this method.[18] For the quantitative comparisons between experiment and simulation for shot 138 038 at $\rho=0.65$, $t=1525$ ms, no such modifications (e.g., to ITG or background $E\times B$ shear) to the GYRO inputs have been made. These types of detailed input sensitivity scans are valuable, but may be bypassed in future work because the use of flux-matched profiles for experiment-simulation comparisons has recently emerged, e.g., through the use of a new transport solver TGYRO.[47] This method will allow for self-consistent evaluation of the sensitivity to input gradients when the transport is stiff and will be pursued for these discharges in the future.

Linear and nonlinear simulation results for the cross-phase angle are not in good agreement for the postexperiment simulations, in contrast to the good agreement observed in the pre-experiment simulations. This may be due to the stronger turbulence drive from increased density and temperature gradients in the experimental cases, as indicated by results from Ref. 14. These plasmas will be studied in future work comparing quasilinear and nonlinear estimates of the cross-phase angle between density and electron temperature fluctuations. The measurements of $\alpha_{n_eT_e}$ can also be compared against the quasilinear estimates contained in theory based transport models such as TGLF.[15]

Experimental paths forward should focus on exploiting the new $\alpha_{n_eT_e}$ measurement capability at DIII-D. For the turbulence measurements, although there is experimental[27,28] and modeling evidence[29] that the reflectometer amplitude signal contains local information about density fluctuations, most models used to interpret reflectometer density fluctuation data consider only the reflectometer phase signal.[26] Detailed modeling of the reflectometer data from this experiment using 2D full wave codes can be used to study the reflectometer amplitude signal. Similar to work done by Ref. 28, the reflectometer data can be quantitatively compared with BES measurements. It would be useful to use GYRO calculated density fluctuations as the input to the reflectometer full wave codes. In addition to turbulence, the cross-phase angle for coherent and quasicoherent modes, such as reversed shear AEs,[48] neoclassical tearing modes or the edge harmonic oscillation observed during quiescent H-mode plasmas[49] may be measured and compared with theory.

The simultaneous measurements of two-field fluctuation levels, $\tilde{T}_e/T_e$ and $\tilde{n}/n$, and the cross-phase angle $\alpha_{n_eT_e}$ presented here will allow for more rigorous testing of turbulence-transport models contained in nonlinear, gyrokinetic turbulence simulations. The new experimental data set described here allows for detailed code comparisons at mul-

tiple levels of a "primacy hierarchy."[17,18] Toward this goal, a first step will be to complete nonlinear simulations of the experimental "Base" case discharge 138 040 at $\rho=0.65$ to complement the simulations of the "High T_e" discharge, 138 038, that were described in Sec. IV. Followed by this, it is essential to perform nonlinear simulations for both the experimental "Base" case and "High T_e" case at $\rho=0.75$ because this is the radial location no change in the cross-phase angle outside experimental error bars was observed experimentally. Future work will focus on comparing the different responses in the cross-phase angle across the radius with turbulence simulations, which will critically test the codes. Detailed assessments of uncertainties in the experiment and simulations will also be explored as part of applying "validation metrics" to determine relative importance of agreements and disagreements across multiple parameters.[18]

ACKNOWLEDGMENTS

This research was supported by the U.S. Department of Energy under Grant Nos. DE-AC05-06OR23100, DE-FG03-08ER54984, DE-FG02-07ER54917, DE-FG03-95ER54309, and DE-FC02-04ER54698. The research of A.E.W. was performed under an appointment to a DOE ORISE FES postdoctoral fellowship. J.C.H. is supported by a DOE ORISE FES graduate fellowship. A.E.W. wishes to thank the tokamak operators for this experiment, J. R. Ferron and B. Hudson, and would like to acknowledge insightful input from D. Mikkelson and R. Prater. A.E.W. also thanks R. J. Groebner for CER analysis and C. Holcomb for MSE analysis. We thank the entire DIII-D team for their support of these experiments. The GYRO simulations reported here were performed on FRANKLIN at NERSC.

[1] A. J. Wooton, B. A. Carreras, H. Matsumoto, K. McGuire, W. A. Peebles, Ch. P. Ritz, P. W. Terry, and S. J. Zweben, Phys. Fluids B **2**, 2879 (1990).
[2] G. R. Tynan, A. Fujisawa, and G. R. McKee, Plasma Phys. Controlled Fusion **51**, 113001 (2009).
[3] J. C. Foster, P. M. Schoch, and R. L. Hickok, IEEE Trans. Plasma Sci. **22**, 399 (1994).
[4] H. T. Evesen, R. J. Fonck, S. F. Paul, G. Rewoldt, S. D. Scott, W. M. Tang, and M. C. Zarnstoff, Nucl. Fusion **38**, 237 (1998).
[5] M. Häes, M. Hirsch, and H. J. Hartfuss, Rev. Sci. Instrum. **70**, 1014 (1999).
[6] J. L. Luxon, Nucl. Fusion **42**, 614 (2002).
[7] A. E. White, L. Schmitz, W. A. Peebles, T. A. Carter, T. L. Rhodes, E. J. Doyle, P. A. Gourdain, J. C. Hillesheim, G. Wang, C. Holland, G. R. Tynan, M. E. Austin, G. R. McKee, M. W. Shafer, K. H. Burrell, J. Candy, J. C. DeBoo, R. Prater, G. M. Staebler, R. E. Waltz, M. A. Makowski, and DIII-D Team, Rev. Sci. Instrum. **79**, 103505 (2008).
[8] G. R. McKee, R. Ashley, R. Durst, R. Fonck, M. Jakubowski, K. Tritzz, K. Burrell, C. Greenfield, and J. Robinson, Rev. Sci. Instrum. **70**, 913 (1999).
[9] A. E. White, L. Schmitz, G. R. McKee, C. Holland, W. A. Peebles, T. A. Carter, M. W. Shafer, M. E. Austin, K. H. Burrell, J. Candy, J. C. DeBoo, E. J. Doyle, M. A. Makowski, R. Prater, T. L. Rhodes, G. M. Staebler, G. R. Tynan, R. E. Waltz, and G. Wang, Phys. Plasmas **15**, 056116 (2008).
[10] L. Schmitz, G. Wang, J. C. Hillesheim, T. L. Rhodes, W. A. Peebles, A. E. White, L. Zeng, T. A. Carter, and W. Solomon, Rev. Sci. Instrum. **79**, 10F113 (2008).
[11] J. C. Hillesheim, W. A. Peebles, T. L. Rhodes, L. Schmitz, T. A. Carter, P.-A. Gourdain, and G. Wang, Rev. Sci. Instrum. **80**, 083507 (2009).
[12] W. Horton, Rev. Mod. Phys. **71**, 735 (1999).
[13] G. M. Staebler (private communication).
[14] R. E. Waltz, A. Casati, and G. M. Staebler, Phys. Plasmas **16**, 073203 (2009).
[15] J. E. Kinsey, G. M. Staebler, and R. E. Waltz, Phys. Plasmas **15**, 055908 (2008).
[16] J. Candy and R. E. Waltz, J. Comput. Phys. **186**, 545 (2003).
[17] P. W. Terry, M. Greenfield, J.-N. Leboeuf, G. R. McKee, D. R. Mikkelson, W. M. Nevins, D. E. Newman, and D. P. Stotler, Phys. Plasmas **15**, 062503 (2008).
[18] C. Holland, J. Candy, R. Waltz, A. White, G. McKee, M. Shafer, L. Schmitz, and G. R. Tynan, Phys. Plasmas **16**, 052301 (2009).
[19] L. Lin, M. Porkolab, E. M. Edlund, J. C. Rost, C. L. Fiore, M. Greenwald, Y. Lin, D. R. Mikkelsen, N. Tsuji, and S. J. Wukitch, Phys. Plasmas **16**, 012502 (2009).
[20] A. Casati, T. Gerbaid, P. Hennequin, C. Bourdelle, J. Candy, F. Clairet, X. Garbet, V. Grandgirard, O. D. Gürcan, S. Heuraux, G. T. Hoang, C. Honoré, F. Imbeaux, R. Sabot, Y. Sarzin, L. Vermare, and R. E. Waltz, Phys. Rev. Lett. **102**, 165005 (2009).
[21] J. E. Kinsey, R. E. Waltz, and J. Candu, Phys. Plasmas **13**, 022305 (2006).
[22] R. V. Bravenec and W. M. Nevins, Rev. Sci. Instrum. **77**, 015101 (2006).
[23] J. Candy, R. E. Waltz, and W. Dorland, Phys. Plasmas **11**, L25 (2004).
[24] G. M. Staebler, J. E. Kinsey, and R. E. Waltz, Phys. Plasmas **14**, 055909 (2007).
[25] J. S. Bendat and A. G. Piersol, *Random Data* (Wiley, New York, 2000).
[26] R. Nazikian, G. J. Kramer, and E. Valeo, Phys. Plasmas **8**, 1840 (2001).
[27] T. L. Rhodes, W. A. Peebles, E. J. Doyle, P. Pribyl, M. Gilmore, R. A. Moyer, and R. D. Lehmer, Plasma Phys. Controlled Fusion **40**, 493 (1998).
[28] G. Wang, W. Peebles, T. Rhodes, G. Kramer, E. Doyle, G. McKee, R. Nazikian, N. Crocker, X. Nguyen, and L. Zeng, Nucl. Fusion **46**, S708 (2006).
[29] E. Blanco, T. Estrada, and T. Happel, Proceedings of the Ninth International Reflectometry Workshop (IRW9) [Organized in co-operation with the International Atomic Energy Agency (IAEA), 2006].
[30] C. Watts, Fusion Sci. Technol. **52**, 176 (2007).
[31] G. Cima, R. V. Bravenec, A. J. Wootton, T. D. Rempel, R. F. Gandy, C. Watts, and M. Kowon, Phys. Plasmas **2**, 720 (1995).
[32] S. Sattler, H. J. Hartfuss, and W.-A. Team, Phys. Rev. Lett. **72**, 653 (1994).
[33] T. Rempel, A. G. Lynn, P. E. Phillips, and A. Hubbard, Rev. Sci. Instrum. **65**, 2044 (1994).
[34] B. D. Bray, C. Hsieh, T. N. Carlstrom, and C. C. Makariou, Rev. Sci. Instrum. **72**, 1115 (2001).
[35] M. A. Van Zeelannd, R. L. Boivin, T. N. Carlstrom, T. Deterly, and D. K. Finkenthal, Rev. Sci. Instrum. **77**, 10F325 (2006).
[36] M. E. Austin and J. Lohr, Rev. Sci. Instrum. **74**, 1457 (2003).
[37] W. M. Solomon, K. H. Burrell, R. Feder, A. Nagy, P. Gohil, and R. J. Groebner, Rev. Sci. Instrum. **79**, 10F531 (2008).
[38] C. Angioni, A. G. Peeters, G. V. Pereverzev, F. Ryter, G. Tardini, and ASDEX Upgrade Team, Phys. Plasmas **10**, 3225 (2003).
[39] J. A. Boedo, P. Terry, D. Gray, R. Ivanov, S. Conn, S. Jachmich, G. van Oost, and TEXTOR Team, Phys. Rev. Lett. **84**, 2630 (2000).
[40] T. A. Carter and J. E. Maggs, Phys. Plasmas **16**, 012304 (2009).
[41] P. W. Terry, D. E. Newmam, and A. S. Ware, Phys. Rev. Lett. **87**, 185001 (2001).
[42] H. E. St. John, T. S. Taylor, Y. R. Lin-Liu, and A. D. Turnbull, Plasma Phys. Controlled Nucl. Fusion Res. **3**, 603 (1994).
[43] A. W. Leonard, W. H. Meyer, B. Geer, D. M. Behne, and D. N. Hill, Rev. Sci. Instrum. **66**, 1201 (1995).
[44] T. L. Rhodes, W. A. Peebles, X. Nguyen, M. A. Van Zeeland, J. S. deGrassie, E. J. Doyle, G. Wang, and L. Zeng, Rev. Sci. Instrum. **77**, 10E922 (2006).
[45] R. W. Harvey, Bull. Am. Phys. Soc. **39**, 1626 (1994).
[46] R. E. Waltz, J. Candy, and M. Fahey, Phys. Plasmas **14**, 056116 (2007).
[47] J. Candy, C. Holland, R. E. Waltz, M. R. Fahey, and E. Belli, Phys. Plasmas **16**, 060704 (2009).
[48] M. A. Van Zeeland, G. J. Kramer, M. E. Austin, R. L. Bovin, W. W. Heidbrink, M. A. Makowski, G. R. McKee, R. Nazikian, W. M. Solomon, and G. Wang, Phys. Rev. Lett. **97**, 135001 (2006).
[49] K. H. Burrell, W. P. West, E. J. Doyle, M. E. Austin, T. A. Casper, P. Gohil, C. M. Greenfield, R. J. Groebner, A. W. Hyatt, R. J. Jayakumar, D. H. Kaplan, L. L. Lao, A. W. Leonard, M. A. Makowski, G. R. McKee, T. H. Osborne, P. B. Snyder, W. M. Solomon, D. M. Thomas, T. L. Rhodes, E. J. Strait, M. R. Wade, G. Wang, and L. Zeng, Phys. Plasmas **12**, 056121 (2005).